Articles

Application of Turbo Machinery Using Mixed Cooling Gas

OZAKI Shinsuke*

Neon is expected to see growing demand for semiconductor-related applications; however, concerns over supply stability have emerged due to changes in the global situation, making domestic production a key issue. Neon is produced as a by-product of large air separation units, and our company is planning to produce neon using crude neon obtained from the large air separation unit at the Kimitsu Sanso Center.

The cooling system of the neon purification unit consists mainly of turbomachinery (a turbo compressor and an expansion turbine) and heat exchangers. For the turbomachinery, we employ the turbo compressor and expansion turbine of NeoKelvin®-Turbo, which has been commercialized using our refrigeration-cycle and turbomachinery technologies. To prevent liquefaction of the refrigerant and to optimize the turbomachinery design, the cooling system uses a mixed refrigerant of neon gas and helium gas. This paper reports an overview of the cooling system of the neon purification unit and the design and performance of the turbomachinery in the cooling system using the mixed refrigerant.

1. Introduction

Taiyo Nippon Sanso manufactures industrial gases, including oxygen, nitrogen, and argon, and also supplies noble gases such as helium and neon. In recent years, while the demand for noble gases for applications such as semiconductors has been increasing, the supply volume has become unstable due to changes in the global situation. Regarding neon, the entire amount used in Japan is imported from overseas, and domestic production has become an urgent issue to ensure a stable supply. In 2023, with support from the Ministry of Economy, Trade and Industry's project to strengthen the resilience of supply chains for critical materials, we decided to install a neon purification unit at the Kimitsu Sanso Center in Chiba Prefecture[1), 2)].

2. Basic Structure of the Neon Purification Unit

2.1 Overall Process

Fig. 2.1.1 shows the overall process flow of the neon purification unit. Crude neon gas obtained from an air separation unit contains many impurities such as nitrogen, oxygen, hydrogen, helium, and moisture, and the neon concentration is less than 50%. These impurities are removed in the purification system line by oxygen addition, TSA, VPSA, and a cryogenic adsorber, resulting in a mixed gas of helium and neon. Subsequently, the neon concentration is increased in a gas-liquid separator. Then, by cooling the mixed gas to 30 K and performing distillation separation, product neon gas is obtained.

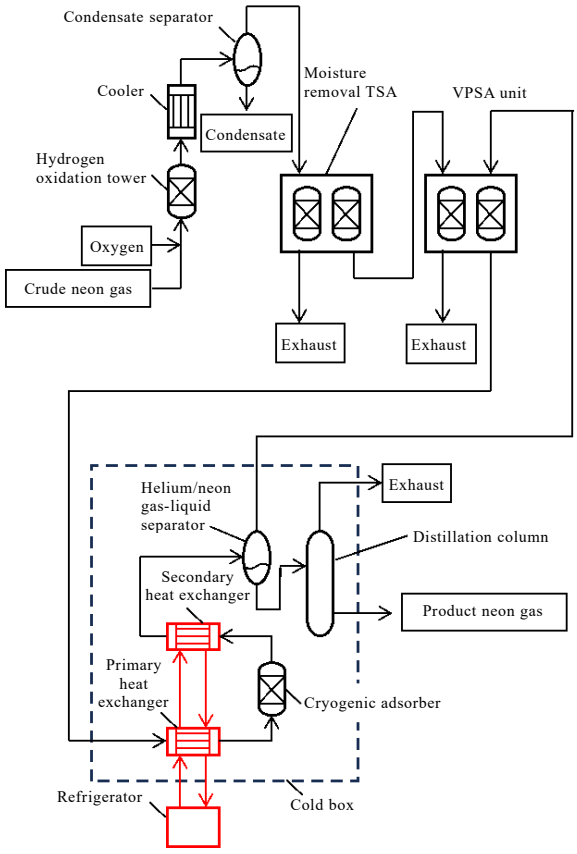

Fig. 2.1.1 Overall process of the neon purification unit

* Technology, Cryogenic Equipment Technology Department, Tsukuba Development Center, R&D Unit

2.2 Cooling System

The cooling system is mainly composed of a turbo compressor, expansion turbines, and heat exchangers, similar to a turbo chiller. The expansion turbines include a warm turbine and a cold turbine[3]. Fig. 2.2.1 shows the schematic flow of the cooling system. The refrigerant is pressurized by the turbo compressor, passes through the heat exchangers, and generates refrigeration by expanding the regrigerant in the warm and cold turbines. Through the heat exchangers arranged on the primary side of each turbine, the warm turbine controls the temperature of crude neon gas entering the cryogenic adsorber, while the cold turbine controls the temperature of crude neon gas entering the neon-helium gas-liquid separator.

For the expansion turbines and turbo compressor used here, in order to shorten the development and manufacturing periods, the aerodynamic components have been redesigned to meet the required specifications of the cooling system based on turbomachinery from turbo chillers.

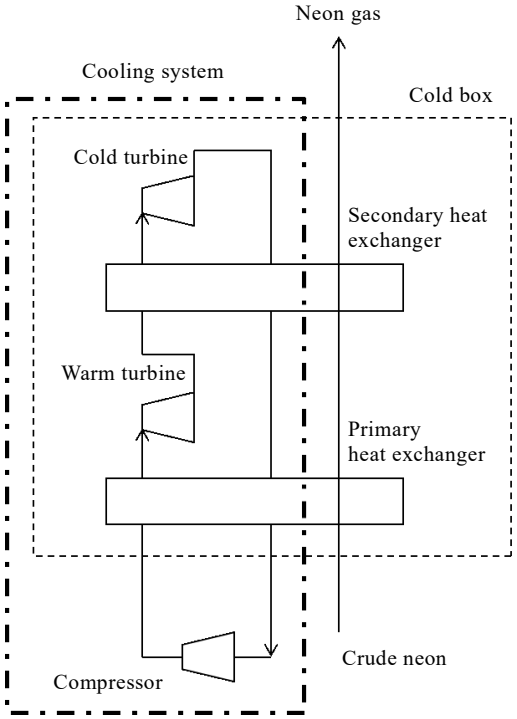

Fig. 2.2.1 Schematic flow of the cooling system

3. Application of Mixed Refrigerant

3.1 Mixing Ratio

Table 3.1.1 shows the required specifications for the cooling temperatures of the warm and cold turbines. While turbo chillers use neon as the refrigerant, the use of a mixed refrigerant of neon and helium was considered for the neon purification unit because there is a concern regarding the liquefaction of neon at the cold turbine outlet.

It is necessary to cool the crude neon to 30 K, and taking into account the temperature difference at the cold end of the heat exchanger, the cold turbine outlet temperature is 27.5 K. Furthermore, considering that the cold turbine outlet temperature fluctuates depending on the operating load, we aimed for design to achieve a refrigerant liquefaction temperature of 25 K or lower.

Fig. 3.1.1 shows a graph of liquefaction temperature with respect to refrigerant type and pressure. It can be seen that the helium concentration must be 50% or higher to keep the liquefaction temperature at 25 K or lower, and that higher helium concentrations make liquefaction less likely to occur even at higher pressures.

Table 3.1.1 Required specifications for turbine outlet temperatures

	Unit	Warm turbine	Cold turbine
Outlet temperature	K	70	27.5

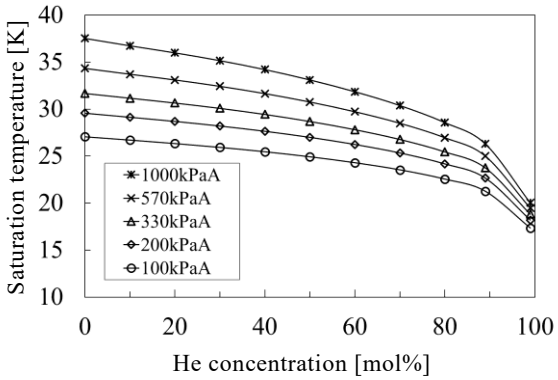

Fig.3.1.1 Liquefaction temperature vs. He concentration

3.2 Turbine Design

Turbine performance has a significant impact on process efficiency within the overall design of the cooling system. Therefore, the turbines were designed to maximize turbine efficiency. One of the performance indicators for turbomachinery is the specific speed N_s, which is expressed by Equation (1).

$$N_s = \frac{n\sqrt{Q}}{H^{0.75}} \quad (1)$$

where N_s is the specific speed [rad/s, m^3/s, J/kg], n is the

rotational speed [rad/s], Q is the refrigerant volume flow rate [m^3/s], and H is the heat drop [J/kg]. For radial turbines, the optimal design range for specific speed is approximately 0.6 to 0.7[5].

Fig. 3.2.1 shows the heat drop with respect to helium concentration and expansion ratio at a turbine inlet temperature of 70 K. The adiabatic heat drop increases as the helium concentration increases or the expansion ratio becomes larger. Here, since the turbines are motor-driven, there is a constraint on the maximum rotational speed. In addition, a helium concentration that prevents refrigerant liquefaction in the cold turbine was adopted. Based on these design conditions, the flow rate and heat drop were determined so that the specific speed falls within the optimal range, and the aerodynamic components were redesigned. Fig. 3.2.2 shows the impeller and nozzle of the warm turbine.

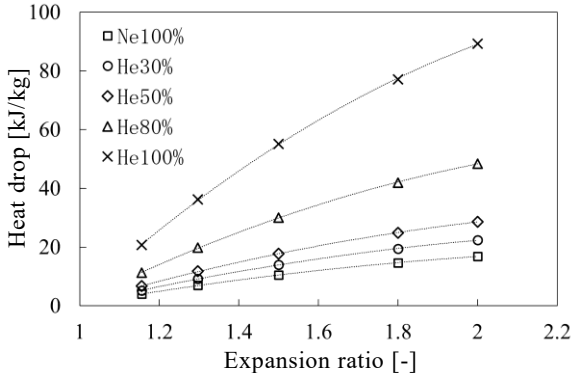

Fig. 3.2.1 Helium concentration vs. adiabatic heat drop

Fig. 3.2.2 Impeller (top) and nozzle (bottom) of the warm turbine

3.3 Turbine Structure and Thermal Insulation Design

On the top of the cold box that accommodates the heat exchangers, the turbine is installed so that the rotating shaft is oriented in the vertical direction. The main shaft to which the impeller is attached is driven by an electric motor and supported by magnetic bearings in the radial and axial directions without contact. Fig. 3.3.1 shows a cross-sectional view of the turbine.

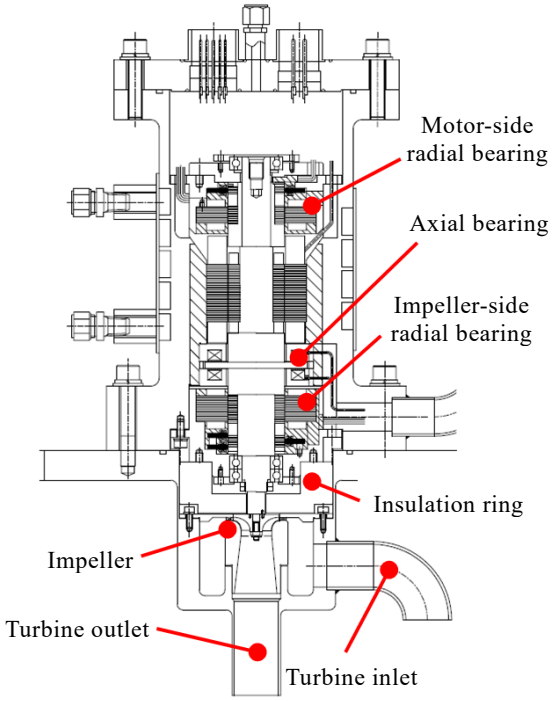

Fig. 3.3.1 Turbine structure

Fig. 3.3.2 shows a structural diagram of the impeller area. While the bearing side is located above the flange of the cold box and remains at room temperature, the impeller side reaches temperatures of 30 K or lower in the case of the cold turbine. Although the casing, which is a pressure-resistant component, is made of metal, it has a thin-walled structure on its side wall. Furthermore, a resin insulation ring with low thermal conductivity is placed between the impeller and the bearing. These insulation structures reduce the heat ingress from the room-temperature side to the cryogenic side, allowing the refrigeration generated by the turbine to be effectively utilized for cooling the crude neon. In addition, the insulation structures prevent the temperature of the bearing from dropping, contributing to improved long-term stability.

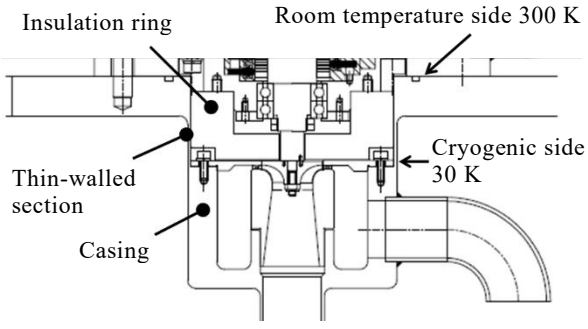

Fig. 3.3.2 Structural diagram of the impeller area

3.4 Turbo Compressor Design

Similar to the turbines, the turbo compressor employs magnetic bearings and an electric motor. Impellers are arranged at both ends of the main shaft, enabling two-stage compression per unit[6]. In the overall design of the cooling system, the turbine was designed first to satisfy the cooling temperature and the required refrigeration. Therefore, the fluid components for the turbo compressor were investigated to satisfy the processing flow rate, pressure ratio, and other requirements of the turbine specifications. In a mixed refrigerant of neon and helium, as the helium concentration increases, the pressure ratio achieved by the turbo compressor decreases due to the reduction in density. Therefore, we redesigned the conventional turbo compressor impeller by increasing its diameter to ensure that the design pressure ratio can be obtained with a helium-mixed refrigerant. Fig. 3.4.1 shows the turbo compressor impeller.

Fig. 3.4.1 Turbo compressor impeller

4. Performance Acquisition

4.1 Turbine Bearing Temperature

To evaluate the integrity of the bearings in the operating states of the warm and cold turbines, the bearing temperatures were measured with respect to the turbine outlet temperature and turbine rotational speed. For the bearing temperature measurement, resistance temperature detectors installed near the electromagnetic coils inside the magnetic bearing units were used.

Fig. 4.1.1 shows the bearing temperature with respect to the turbine outlet temperature. When the turbine outlet temperature was 40 K, the bearing temperature varied with the rotational speed, reaching 30°C at 0.8 times the rated speed and 70°C at 1.1 times the rated speed. On the other hand, it was found that when the rotational speed remains constant at 1.1 times the rated speed, the bearing temperature is maintained constant even if the cooling temperature changes between 40–70 K.

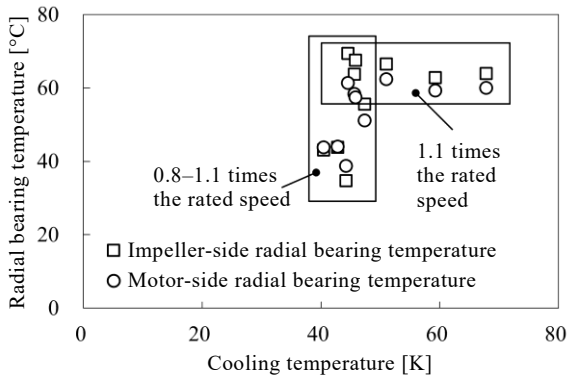

Fig. 4.1.1 Turbine bearing temperature

4.2 Warm Turbine Efficiency

Fig. 4.2.1 shows the test flow for the performance evaluation of the warm turbine. The refrigerant pressurized by the turbo compressor is cooled by the heat exchanger and supplied to the turbine. The expansion ratio of the turbine was adjusted by the rotational speed of the turbo compressor, and the turbine inlet pressure was adjusted by supplying and recovering refrigerant from the buffer tank. The turbine inlet temperature was controlled by the output of a film heater attached to the surface of the heat exchanger. The turbine inlet temperature was maintained at 70 K, which is the warm turbine specification.

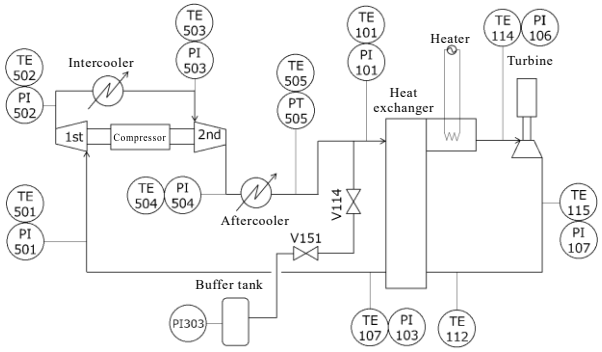

Fig. 4.2.1 Test flow

Turbine efficiency is shown in Equation (2).

$$\eta = \frac{(H_0 - H_2)}{(H_0 - H_{2i})} \tag{2}$$

where H_0 is the turbine inlet enthalpy, H_2 is the turbine outlet enthalpy, and H_{2i} is the turbine outlet enthalpy in the case of ideal adiabatic expansion between the turbine inlet and outlet. Since losses occur due to separation and friction in the fluid at the turbine inlet and outlet, the turbine efficiency does not reach 100%. $U/C0$ is called the velocity ratio, where U is the peripheral speed of the impeller's outer diameter and $C0$ is the theoretical adiabatic spouting velocity, which represents the adiabatic heat drop between the turbine inlet and outlet in terms of velocity. In general, the maximum efficiency of a turbine is obtained when $U/C0$ is around 0.7[7].

Fig. 4.2.2 shows the efficiencies of a turbo chiller turbine and the warm turbine. Within the measured range of U/C0, the warm turbine achieved an efficiency 5 points higher than the required specifications. Also, the efficiency of the warm turbine was equivalent to that of the turbo chiller turbine.

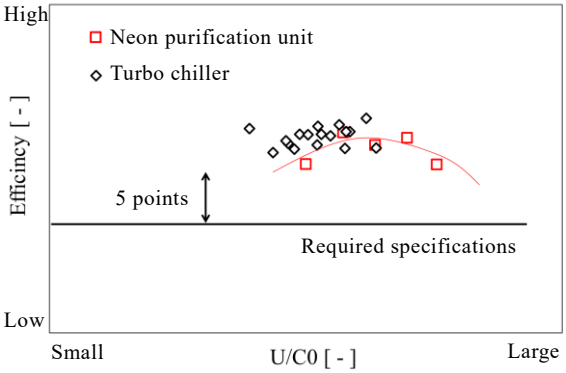

Fig. 4.2.2 Warm turbine efficiency

4.3 Consideration of Generated Refrigeration and Turbine Efficiency

This section considers the influence of heat ingress from the room-temperature section and the magnitude of the refrigeration generated by the turbine on changes in efficiency. Fig. 4.3.1 represents the changes between the turbine inlet and outlet in terms of entropy and enthalpy. Taking H_0 as the turbine inlet enthalpy, if the refrigerant expands ideally, the expansion is an isentropic process, and the turbine outlet enthalpy becomes H_{2i}. Various losses occur in reality, so the expansion is not an isentropic process, and the outlet enthalpy becomes H_2; thus, the turbine efficiency η is expressed by Equation (2).

Here, the measured turbine efficiency η is considered to be lower than it would be without heat ingress, as the heat ingress q from the casing and insulation shown in Fig. 3.3.2 causes the turbine outlet temperature to rise. In this case, considering the scenario without heat ingress q, the turbine outlet temperature becomes T_q, and the turbine efficiency without heat ingress η_q is given as follows.

$$\eta_q = \frac{(H_0 - H_q)}{(H_0 - H_{2i})} \tag{3}$$

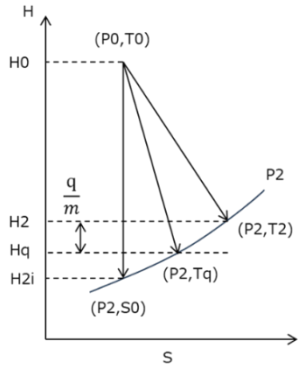

Fig. 4.3.1 Turbine efficiency

The generated refrigeration Q with heat ingress is expressed by Equation (4), and the heat ingress q is expressed by Equation (5).

$$Q = \dot{m}(H_0 - H_2) \quad (4)$$

$$q = \dot{m}(H_2 - H_q) \quad (5)$$

where $\dot{m}$ [kg/s] is the mass flow rate.

Therefore, the relationship between the measured turbine efficiency η and the turbine efficiency without heat ingress η_q is expressed by Equation (6) using the generated refrigeration Q and heat ingress q.

$$\eta = \frac{(H_0 - H_2)}{(H_0 - H_{2i})}$$

$$= \frac{H_0 - \left(H_q + \frac{q}{\dot{m}}\right)}{(H_0 - H_{2i})}$$

$$\eta = \eta_q \frac{Q}{Q+q} \quad (6)$$

Equation (6) shows that even if the heat ingress is the same, the turbine efficiency varies depending on the amount of generated refrigeration. Since the insulation structures of the warm turbine and a turbo chiller turbine are the same, the heat ingress is considered to be equivalent. Here, the change in efficiency based on the ratio of heat ingress to the generated refrigeration is considered as follows. Table 4.3.1 compares the turbine efficiency η_q for cases where the turbine efficiency η is 70%, the heat ingress is 1, and the generated refrigeration is 10, 20, and 30 times the heat ingress. Since the neon purification unit corresponds to Case 1, and turbo chillers correspond to Case 2 or Case 3, the Table shows that, if heat ingress is not taken into account, the warm turbine efficiency is improved by approximately 4% compared to the turbo chiller turbine. Therefore, it was found that the fluid components achieved higher efficiency through the redesign.

Table 4.3.1 Relationship between generated refrigeration, heat ingress, and turbine efficiency

	Unit	Case 1	Case 2	Case 3
Heat ingress	-	1	1	1
Generated refrigeration	-	10	20	30
Efficiency η	%	70	70	70
Efficiency η_q	%	77	73.5	72.3

4.4 Turbo Compressor Performance

Fig. 4.4.1 shows the results for the flow rate and pressure ratio of the turbo compressor. The turbo chiller compressor had an insufficient pressure ratio at the specified flow rate. The neon purification turbo compressor successfully met the required specifications as the pressure ratio was increased by expanding the impeller diameter. However, since the operating range on the low flow rate side became narrower and more prone to surging, the necessity of anti-surging measures for the actual unit was clarified.

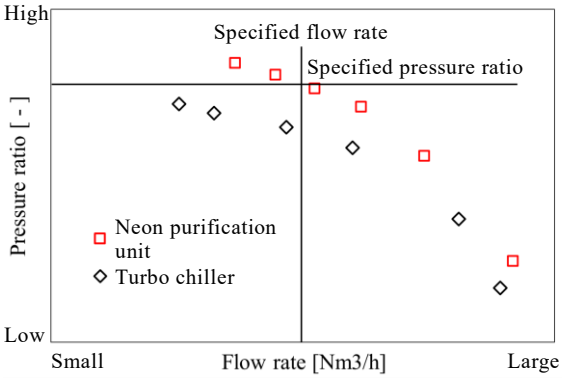

Fig. 4.4.1 Flow rate and pressure ratio

5. Conclusion

To achieve the early realization of a cooling system for neon purification units, we conducted an application study and evaluation of expansion turbines and turbo compressors for our internally developed turbo chillers. By applying the concept of the patent we obtained in 2021 regarding mixed refrigerants, we confirmed that it is possible to achieve a warm turbine efficiency equivalent to that of turbo chiller turbines while preventing refrigerant liquefaction[8].

We investigated the influence of the refrigeration generated by the turbine and the heat ingress into the cryogenic side on the turbine efficiency, and formulated their relationship. As a result, it has become possible to

quantitatively evaluate the decrease in efficiency caused by generated refrigeration and heat ingress. These findings can also be applied to expansion turbines for air separation units our company handle.

If local production for local consumption of neon is realized through domestic manufacturing, the energy required for its transportation will be reduced, and its stable supply will also be achieved. By applying our technologies in refrigeration cycles and turbomachinery, we will continue to actively work toward solving social issues.

References

1) Taiyo Nippon Sanso Corporation News Release (regarding neon production): https://www.tn-sanso.co.jp/LinkClick.aspx?fileticket=wW563uc705s%3D&tabid=207&mid=952
2) Ministry of Economy, Trade and Industry (METI) (regarding neon gas production): https://www.meti.go.jp/information_2/publicoffer/review2025/kokai/0606_1gaiyo.pdf
3) Taiyo Nippon Sanso Corporation News Release "Launch of Sales of the World’s First Turbo Refrigerator for Cooling Superconducting Power Equipment," https://www.tn-sanso.co.jp/LinkClick.aspx?fileticket=3R0gULrYchI%3D&tabid=207&mid=952
4) Taiyo Nippon Sanso CSR Report 2025 p. 9 https://www.nipponsanso-hd.co.jp/Portals/0/images/csr/shareholders/kankyo2015.pdf
5) M. Ishii et al., "Utilizing of Mixture Refrigerant in Brayton Cycle Using Turbomachinery," Taiyo Nippon Sanso Technical Report, 2022, no. 41, pp. 13-18.
6) K. Hirai et al., "Development of a Small Turbo-Compressor with Active Magnetic Bearings," Taiyo Nippon Sanso Technical Report, 2010, no. 29, pp. 7-11.
7) David Japikse ets, Axial and Radial Turbines, p. 273
8) Taiyo Nippon Sanso Corporation, "Turbo Brayton Refrigerator," Patent No. 6951598, September 28, 2021.